Estonian Journal of Earth Sciences
2023, **72**, 2, 171–184

https://doi.org/10.3176/earth.2023.83

www.eap.ee/earthsciences
Estonian Academy Publishers

RESEARCH ARTICLE

Received 9 November 2022
Accepted 18 January 2023
Available online 21 September 2023

Keywords:
early Cambrian, Atdabanian, source rocks, trace elements, paleoredox

Corresponding author:
Olev Vinn
olev.vinn@ut.ee

Citation:
Azizi, A., El Albani, A., El Hariri, K., El Bakhouch, A., Vinn, O., Hafid, A. and Kirsimäe, K. 2023. Geochemistry of the early Cambrian succession in the western Anti-Atlas, Morocco: implications on provenance and paleoredox conditions. *Estonian Journal of Earth Sciences*, **72**(2), 171–184.
https://doi.org/10.3176/earth.2023.83

Geochemistry of the early Cambrian succession in the western Anti-Atlas, Morocco: implications on provenance and paleoredox conditions

Abdelfattah Azizi[a], Abderrazak El Albani[b], Khadija El Hariri[a], Asmaa El Bakhouch[a], Olev Vinn[c], Ahmid Hafid[a] and Kalle Kirsimäe[c]

[a] Laboratoire de Géoressources, Géoenvironnement et Génie Civil, Département des Sciences de la Terre, Faculté des Sciences et Techniques, Université Cadi-Ayyad, BP 549, 40000 Marrakesh, Morocco

[b] Laboratoire IC2MP 7285 CNRS-INSU, Université de Poitiers, 86022 Poitiers, France

[c] Department of Geology, Institute of Ecology and Earth Sciences, University of Tartu, Ravila 14A, 50411 Tartu, Estonia

ABSTRACT

The Igoudine and Amouslek formations (Terreneuvian–Cambrian Epoch 2 boundary) in the western Anti-Atlas of Morocco record the replacement of stromatolite-dominated microbial consortia by thrombolite-metazoan consortia. Carbonate and calcareous shales of both formations have been analyzed for major, trace, and rare earth elements to study their geochemical characteristics and evaluate the provenance of the terrigenous fraction and paleoredox conditions. Discrimination diagrams for the source rocks based on major elements and selected trace elements indicate that the terrigenous fractions of the sediments were likely derived from predominantly felsic rocks, and the source rocks have been identified to be the Paleoproterozoic–Neoproterozoic granites and metasediments of the Kerdous inlier. Paleoredox proxies such as U/Al, V/Al and Mo/Al suggest that the Igoudine and Amouslek formations were deposited in the oxic environment. Our data show that the local water column was prevailingly oxidized before, during and after the transition from the microbial consortium (stromatolite-dominated biota) to the thrombolite-archaeocyathan consortium and shelly metazoans within the studied interval. This implies that the seawater redox status was not driving this change in these biological communities.

Introduction

The transition from the Proterozoic to the Phanerozoic (ca 1000–500 Ma) was a time of significant and dramatic changes in Earth's geological history, marked by large-amplitude climatic perturbations (Harland 2007; Hoffman et al. 2017), an increasing oxygen level in the atmosphere (Och and Shields-Zho 2012; Alcott et al. 2019), extreme reconstructions in Earth's biogeochemical cycles and disturbances in the carbon cycle (Halverson and Shields-Zhou 2011; Wood et al. 2019), as well as the emergence of the modern multicellular animal life (Butterfield 2015; Narbonne 2005), topped with the explosive animal biodiversification of the Cambrian, termed the "Cambrian explosion" (Brasier 1982; Zhang and Shu 2021). The replacement of the biosphere dominated by microbial consortia by complex metazoan phyla and the development of bioturbation have been recorded in the fossil record worldwide, but the driving forces behind these changes have long been debated (Levinton 2008; Smith and Harper 2013; Zhang and Shu 2021). On the one hand, this period is characterized by the emergence of oxygenated marine water column, which occurred under rapidly fluctuating redox conditions (Tostevin et al. 2019; Wood et al. 2019), while it has been suggested that the Cambrian explosion of metazoans, which started at ca 540 Ma, may have been facilitated by such dynamics in redox conditions (Wood et al. 2019). Therefore, the study of the paleoredox conditions of marine water columns provides us with a better understanding of the driving factors for the Cambrian explosion.

Biotic replacement of microbial consortium (stromatolite-dominated biota) by a thrombolite-archaeocyathan consortium and shelly metazoans in Anti-Atlas successions is recorded in the Igoudine Formation deposited in Adtabanian age (Cambrian Epoch 2) (Hupé 1960; Schmitt and Monninger 1977; Sdzuy 1978; Schmitt 1979; Destombes et al. 1985; Debrenne and Debrenne 1995; Álvaro and Clausen 2006; Álvaro and Debrenne 2010; Clausen et al. 2014; Azizi et al. 2022). At the same time, the earliest appearance of archaeocyaths has been recorded in the Siberian Platform during Terreneuvian Age 2 (Rowland and Shapiro 2002), reaching its maximum diversity and extension during the Cambrian Age 3–4 interval (Clausen et al. 2014). The apparent delayed record of the Cambrian explosion in Moroccan successions has previously been interpreted as complex interactions among biotic and abiotic factors, whereas the main control of the immigration of archaeocyaths and shelly metazoans was the early Cambrian (Cambrian Epoch 2, Age 3) appearance of open-marine conditions, facilitated by differential subsidence of the platform and a long-term sea-level rise (Clausen et al. 2014).

The early Cambrian succession of Morocco is well exposed in the Anti-Atlas belt. During this time, the marine platform of the Anti-Atlas was part of the northern margin of the Gondwana supercontinent. The early Cambrian succession of the western Anti-Atlas has been studied extensively in terms of depositional environments and stratigraphy, using biostratigraphy and stable carbon isotope chemostratigraphy (Hupé 1960; Schmitt and Monninger 1977; Sdzuy 1978; Schmitt 1979; Destombes et al. 1985; Tucker 1986; Debrenne and Debrenne 1995; Geyer and Landing 1995; Benssaou and Hamoumi 2001, 2004; Maloof et al. 2005; Álvaro and Clausen 2006; Álvaro and Debrenne 2010; Álvaro et al. 2014; Clausen et al. 2014). Most of these studies were focused on the successions outcropping on the northern slope of the Anti-Atlas in Tiout, Tazemourte and Amouslek areas. The Igoudine and Amouslek formations of the Fouanou syncline of the Anti-Atlas represent a well-exposed succession covering this important interval in Earth's history. Despite the biogeochemical characteristics of this section, no detailed study has been carried out on the provenance and paleoredox conditions of the sediments.

The aim of this contribution was to reconstruct the provenance of the Amouslek and Igoudine formations exposed in the Fouanou syncline, in the western Anti-Atlas of Morocco, as well as to interpret the paleoredox conditions surrounding the Tommotian–Atdabanian boundary interval (Terreneuvian–Cambrian Epoch 2), using major and trace element geochemistry of these sediments to examine the role of paleoredox in controlling the faunal evolution of the Sous Basin.

Geological setting

The Anti-Atlas Mountains form a NE-SW trending belt, located in central Morocco (Fig. 1A). It is bounded in the north by the South Atlas Fault (SAF), and in the south by the Tindouf Basin. The northern margin of the West African Craton (WAC) crops out in several massifs and inliers of Paleoproterozoic–Neoproterozoic age, including from west to east the Bas Drâa, Ifni, Kerdous, Akka, Igherm, Siroua, Zenaga, Bou Azzer-El Graara, Saghro and Ougnate inliers (Fig. 1B). The Precambrian rocks of Pan-African orogeny of the Anti-Atlas were covered by the Paleozoic sedimentary rocks that are exposed in the southern slope of the Anti-Atlas (Destombes et al. 1985; Geyer and Landing 1995). The lower Cambrian succession exposed in the western Anti-Atlas (Sous Basin) overlies the Ediacaran Ouarzazate Supergroup

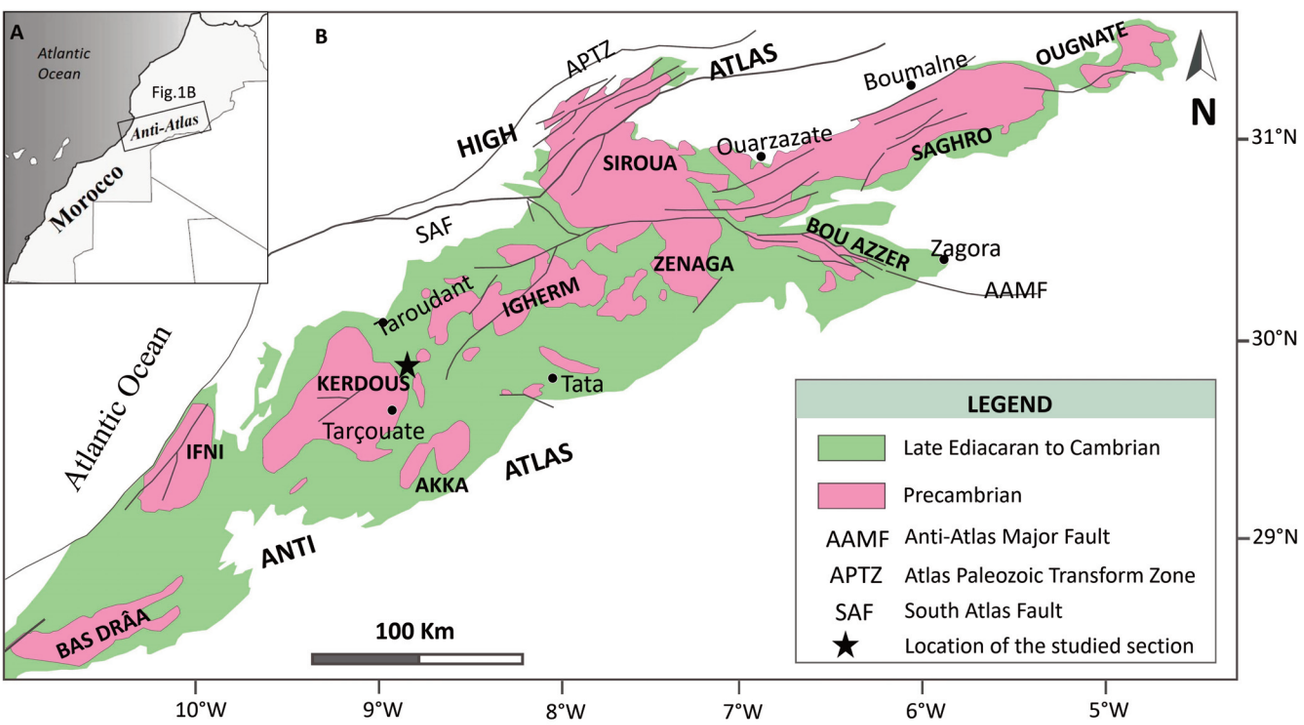

Fig. 1. **A** – location of the Anti-Atlas Mountains. **B** – simplified geological scheme showing the distribution of Ediacaran–Cambrian outcrops in the Anti-Atlas (modified after Saadi et al. 1985).

(Thomas et al. 2002, 2004) and is composed of volcanic and volcanosedimentary rocks (up to 2 km in thickness) deposited in fluvial sedimentary environments (Thomas et al. 2002; Gasquet et al. 2005, 2008; Walsh et al. 2012).

The lower Cambrian succession of the Anti-Atlas was subdivided into two extended groups: the Taroudante and Tata groups (Fig. 2A), both of which formed the early Cambrian carbonate platform which was dominated by dolomites and calcareous sediments developed in the western margin of Gondwana (Álvaro et al. 2003). The Taroudant Group (1000 m thick) comprises two formations: the Adoudou and the Lie-de-vin formations (Fig. 2A). The Adoudou Formation was

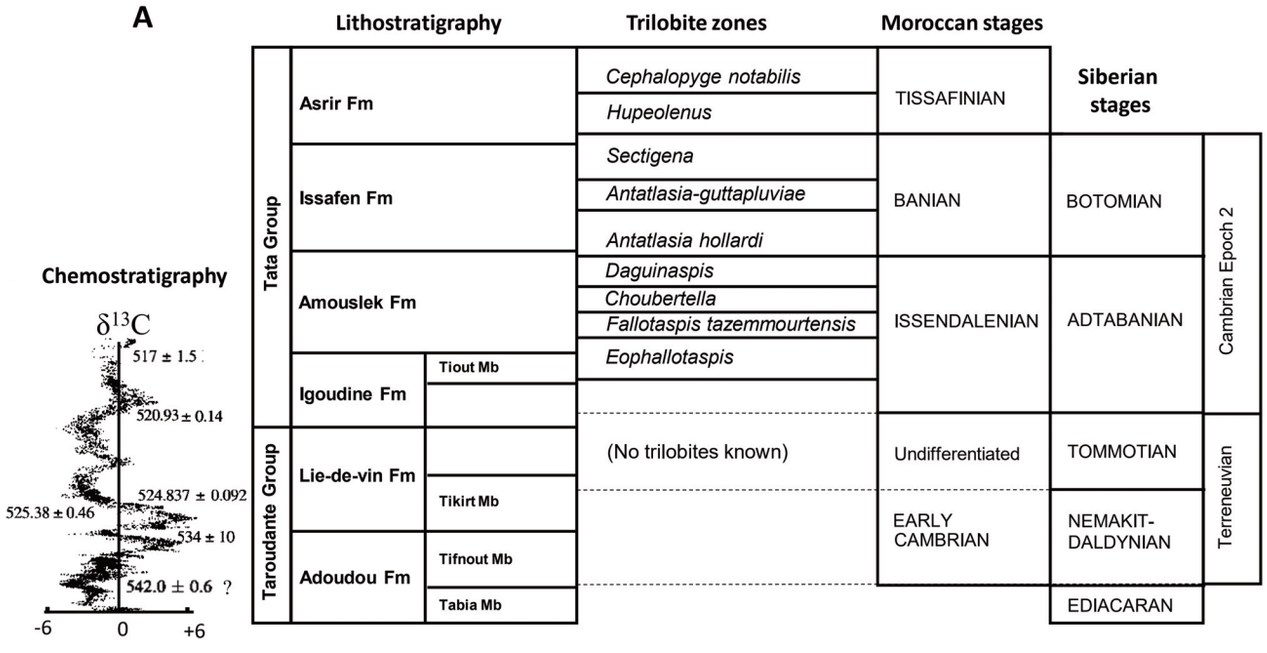

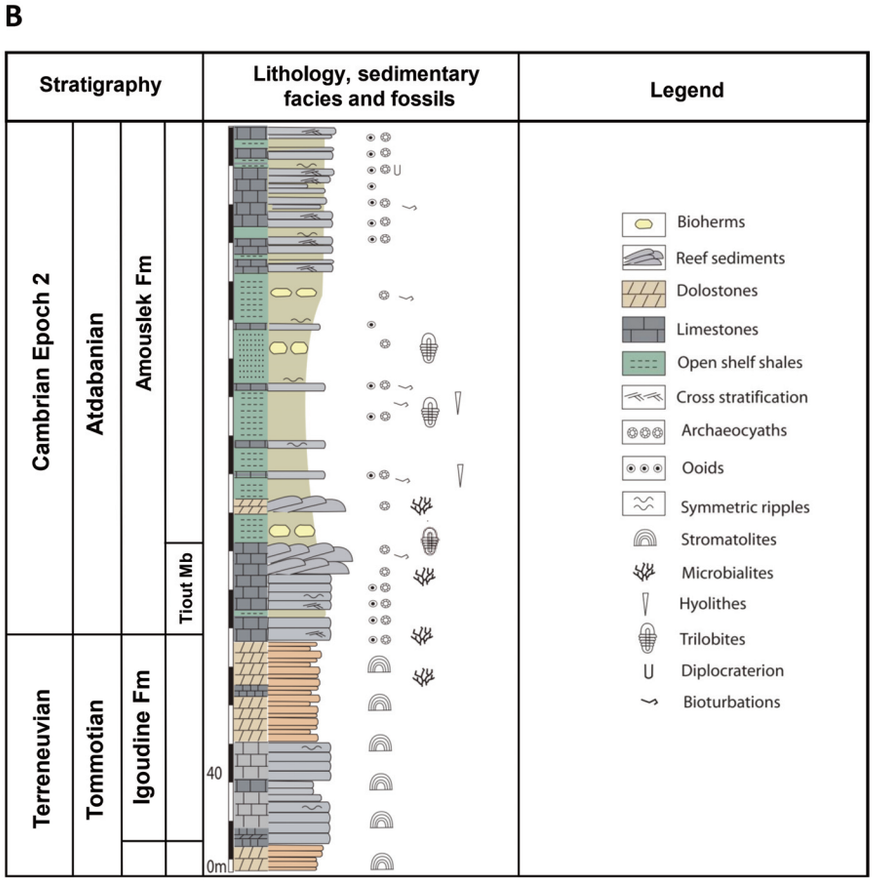

Fig. 2. **A** – Neoproterozoic–Lower Cambrian stratigraphy of the Amouslek–Tiout area (modified after Geyer et al. 1995; Alvaro et al. 2006, 2014), $\delta^{13}C$ chemostratigraphy from Maloof et al. (2005). **B** – lithological column of the studied lower Cambrian section in the Fouanou syncline. Fm – Formation, Mb – Member.

also subdivided into two units by Choubert (1952). The lower unit was named *la série de base* (Tabia Member sensu Maloof et al. 2005) (up to 150 m thick), overlain by the upper unit named as *les calcaires inférieures* by Choubert (1952) (Tifnout Member sensu Maloof et al. 2005), with a thickness ranging from 200 to 1000 m. This upper unit consists of massive to bedded stromatolitic dolostones (Buggisch and Heinitz 1984; Buggisch and Flügel 1988; Álvaro et al. 2000). A chemostratigraphic study of $\delta^{13}C$ by Maloof et al. (2005) (Fig. 2A) suggests an age of 542.0 Ma for the bottom of the Adoudou Formation, based on the correlation of the –6‰ $\delta^{13}C$ excursion, with the negative excursion recorded worldwide at the Ediacaran–Cambrian boundary (Grotzinger and Knoll 1995; Knoll and Carroll 1999; Kimura and Watanabe 2001; Amthor et al. 2003). Furthermore, the minimum radiometric age was established by Ducrot and Lancelot (1977) for the lower Tifnout Member (Taroudante Group) with a U-Pb date of 534 ± 10 Ma obtained on zircons from the Jbel Boho volcano, in the Alougoum area. The carbonate sediments of the Tifnout Member are overlain by the regressive siliciclastic fine-grained sediments of the Lie-de-vin Formation, the thickness of the latter unit reaching ~900 m toward the central Anti-Atlas. In the western Anti-Atlas, this formation is dominated by dolostone and limestone rocks rich in stromatolites and thrombolites (Gayer and Landing 1995; Benssaou and Hamoumi 2001, 2004).

The Tata Group (~1000 m thick) is exposed in the western Anti-Atlas Sous Basin, and was described mainly in the Taroudante area, in Tiout, Amouslek, Tazemmourt type sections (Álvaro and Clausen 2006) and within the Issafen and Fouanou synclines (Benssaou and Hamoumi 2001, 2004). The Tata Group is subdivided into four formations: Igoudine, Amouslek, Issafen and Asrir formations (Fig. 2A). The Igoudine Formation, *calcaires supérieures* in Choubert (1952), consists mainly of dolomitized limestones (dominant in the lower part) and massive to bedded black oolithic limestones. The latter is overlain by the fossiliferous Tiout Member. This unit contains the first indication of the transition from microbial consortia (stromatolite-dominated) to shelly metazoan-thrombilite consortia, rich in fossils of Atdabanian age, such as archaeocyaths, chancelloriids, hyoliths, calcimicrobes and trilobites (Hupé 1960; Sdzuy 1978; Debrenne and Debrenne 1995; Álvaro and Clausen 2006; Álvaro and Debrenne 2010; Azizi et al. 2022). The Amouslek Formation ranges in thickness from 20 to 220 m and consists mainly of variegated shales interbedded with black oolithic limestones bearing small-sized archaeocyaths. The Amouslek Formation is overlain by the fossiliferous Issafen Formation (~400 m thick) consisting of green shale interbedded with nodular limestone, microbial-archaeocyathan bioherms, biostromes and numerous mud-mound complexes (Álvaro and Debrenne 2010).

Materials and methods

The Tommotian–Atdabanian (Terreneuvian–Cambrian Epoch 2) boundary interval was sampled in the Fouanou syncline (NE-SW trend) in the western Anti-Atlas (Figs 1B and 2B), located between the Igherm and Kerdous inliers.

Altogether 18 samples were taken for determining the chemical and mineral composition. The outer weathered surface layer of the outcrop samples was removed and only the inner unweathered part was sampled. Major, trace, and rare earth element (REE) concentrations were analyzed by inductively coupled plasma mass and optical emission spectrometry (ICP-MS, ICP-OES) in Li-borate fused beads dissolved in an HNO_3 (1 mol/L)-H_2O_2 (0.5%)-glycerol (10%, vol/vol) mixture. The trace element (including the REE) concentrations were measured by Thermo × 7 ICP-MS. The major elements were determined by Thermo iCap6500 ICP-OES. The analytical precision of the studied samples was better than 10%. The REE concentrations were normalized relative to the Post Archean Australian Shale (PAAS) values (Taylor and McLennan 1985). La, Ce, and Eu anomalies were calculated as geometric averages (Lawrence et al. 2006).

The whole-rock mineralogy was obtained from powdered, unoriented samples by means of X-ray diffraction (XRD). The XRD patterns were measured using a Bruker D8 Advance diffractometer in the range of 2–70° 2θ. The quantitative mineralogical compositions were interpreted and modeled using the Rietveld algorithm-based program Topas 4 by Bruker. The relative error for major mineral components (>5 wt%) was ~10%, and ~20% for minor mineral components (<5 wt%).

Results

Sedimentary facies

The studied section comprises the Igoudine and Amouslek formations (Fig. 2B). Both formations show sedimentary facies similar to that described in the stratotypic Tiout and Amouslek areas (Álvaro and Clausen 2006; Álvaro and Debrenne 2010; Azizi et al. 2022). The lowermost part of the Igoudine Formation (~40 m thick) is dominated by massive black oolithic limestones, symmetric ripples, cross stratifications and rare dome-shaped stromatolites. The middle part (~30 m thick) consists of massive stratified dolostones, displaying crinkled, stratiform and dome-shaped stromatolites, wave ripples, and rare cross stratifications. Some parasequences show faulted and overturned stromatolites, indicating an episodical instability and slumping of the seafloor. Based on the sedimentary facies analysis, the Igoudine Formation was deposited in the upper subtidal to intertidal environment. The topmost part of the Igoudine Formation is represented by "black oolitic limestone" of Schmitt (1979) consisting of massive, bedded oolitic limestone. This unit records the first appearance of small-sized archaeocyathan cups, dominantly characterized by irregular forms typically preserved in life position. Some beds exhibit erosional surfaces, cross-bedding and wave ripples. This unit is overlain by the first archaeocyathan-microbial reef complex (~30 m thick) distinguished as the Tiout Member of the Igoudine Formation, dominated by dendritic microbialites embedding archaeocyaths. Archaeocyathan cups are typically preserved in life position. The overlying Amouslek Formation is domi-

nated by shales and siltstones, recording a rapid sea-level change from shallow marine restricted conditions to deeper marine conditions (Álvaro and Debrenne 2010; Azizi et al. 2022). The lower interval of this unit contains numerous archaeocyathan-microbial bioherms and isolated patch reefs. The upper interval is dominated by shales and interbedded oolitic limestones, rare fine-grained sandstones beds, wave ripples and cross stratification, recording alternating transgressive-regressive sequences.

Mineral composition and major elements

The mineral composition of the limestone-dolomite succession of the Igoudine Formation is characterized by an interlayering of beds dominated by calcite or dolomite with small amounts of a quartz, K-feldspar, plagioclase, and phyllosilicate (chlorite and K-mica) assemblage (Fig. 3). The content of calcite or dolomite reaches > 80 wt% in carbonate beds (in most of the sampled beds typically >95 wt%). The content of non-carbonate phases is low (in most cases <10 wt%) and is mainly represented by quartz and minor phyllosilicates (K-mica and chlorite). The lower part of the Amouslek Formation represented by shales and siltstones is characterized by quartz–feldspar (mainly plagioclase) and phyllosilicate assemblages (Fig. 3). The quartz content in shale-siltstone-sandstone beds varies from 27 to nearly 45 wt%, whereas feldspars and phyllosilicates constitute up to 44 wt% and 57 wt%, respectively. The carbonate beds in the upper part of the studied section are composed of calcite (>85 wt%) and subdued amounts of dolomite (<11 wt%) with minor quartz, feldspar, and phyllosilicates (Fig. 3).

The major element compositions of the studied samples from Igoudine and Amouslek formations are shown in Table 1. The Igoudine carbonate rocks have a lower SiO_2 content between 0.97 and 7.91 wt%, whereas the Amouslek calcare-

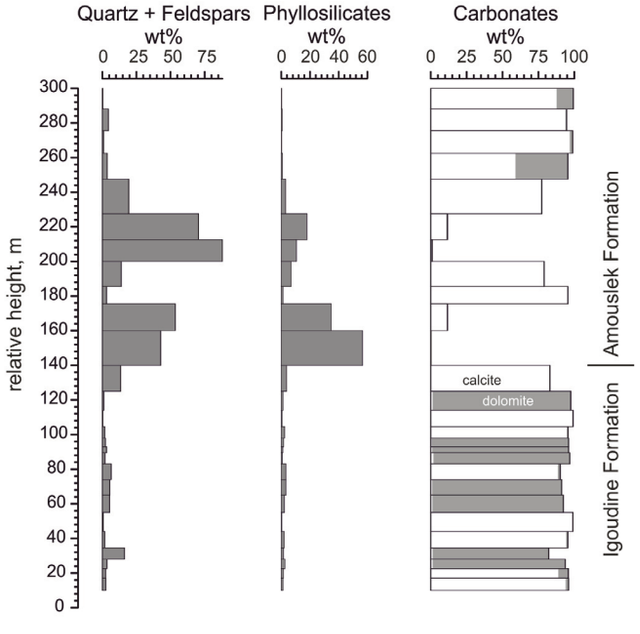

Fig. 3. Mineral composition of the studied samples. Quartz + feldspars (quartz, K-feldspar, plagioclase), phyllosilicates (K-mica, chlorite), carbonate (calcite, dolomite). Calcite content is shown with white bars and dolomite content with gray bars.

Table 1. Major element concentrations (wt%) for the Igoudine and Amouslek formations

Samples	Ig 1	Ig 2	Ig 3	Ig 4	Ig 5	Ig 6	Ig 7	Ig 8	Ig 9	Ig 10	Am 1	Am 2	Am 3	Am 4	Am 5	Am 6	Am 7	Am 8
SiO_2	2.38	4.17	2.86	1.72	5.88	7.52	7.91	2.40	2.77	0.97	13.09	60.79	57.19	12.89	77.65	16.22	1.88	1.25
Al_2O_3	0.21	0.68	0.60	0.19	0.76	1.42	1.29	0.19	0.71	0.10	2.76	17.66	14.19	3.33	11.10	3.72	0.18	0.42
Fe_2O_3	0.07	0.51	0.30	0.11	0.94	0.59	0.34	0.40	0.72	0.06	0.62	5.95	5.20	1.11	1.73	0.84	0.21	0.50
MnO	0.01	0.02	0.01	0.01	0.02	0.04	0.01	0.05	0.04	0.01	0.05	0.01	0.02	0.10	0.11	0.24	0.04	0.05
MgO	0.83	20.16	0.74	0.76	19.82	18.64	0.88	20.10	20.23	0.32	0.82	3.53	3.07	1.17	0.52	0.79	1.06	3.01
CaO	53.03	28.97	52.31	53.59	28.43	28.53	49.24	29.79	29.46	54.49	44.62	0.54	6.25	43.61	0.61	41.98	52.62	50.27
Na_2O	–	0.03	–	–	0.02	0.04	–	0.04	0.04	–	0.90	0.98	2.26	0.98	4.29	1.65	–	0.01
K_2O	0.07	0.14	0.09	0.14	0.15	0.22	0.14	0.07	0.15	0.01	0.65	5.51	3.51	0.56	1.85	0.44	0.11	0.13
TiO_2	0.01	0.02	0.03	0.01	0.02	0.06	0.05	0.01	0.03	–	0.11	0.77	0.60	0.13	0.42	0.16	0.01	0.02
P_2O_5	–	–	–	–	–	–	–	–	–	–	0.05	0.17	0.16	0.05	0.19	0.05	–	–
Al_2O_3/TiO_2	23.00	33.90	23.04	24.13	39.84	24.84	26.24	23.75	25.43	25.75	25.07	22.93	23.73	24.88	26.29	23.38	20.44	22.32

Ig – Igoudine, Am – Amouslek.

ous shales show a high content of SiO_2 ranging from 1.25 to 77.65 wt%. The Al_2O_3 content shows moderate variations in Igoudine samples (0.19–1.42 wt%), but the variation is large (1.25–60.79 wt%) in the overlying Amouslek calcareous shales. The CaO content of the samples varies between 0.54 and 6.25 in shales-siltstones and reaches 54.49 wt% in limestones. The Amouslek samples are enriched in TiO_2, which has a range between 0.004 and 0.77 wt%. The P_2O_5 was above the detection limit only in Amouslek calcareous shales with a maximum value of 0.19 wt%. The MgO concentrations are, as expected, the highest in dolomitic samples, reaching 20.23 wt%, and the lowest in siltstone samples (0.32 wt%). The K_2O content varies from 0.01 to 5.51 wt%, Na_2O from 0.01 to 4.29 wt%, Fe_2O_3 from 0.06 to 5.95 wt%, and MnO from 0.0075 to 0.24.

Trace elements and rare earth elements

The trace element and REE composition of the Igoudine and Amouslek formations is shown in Table 2 and Figs 4–7. The Igoudine carbonates are depleted in trace elements, except in Sr, which probably resides in carbonate minerals (calcite and/or dolomite). Similarly, trace element concentrations are low in pure carbonate beds of the Amouslek Formation, whereas trace element concentrations in calcareous shales in the lower part of the Amouslek Formation are somewhat higher and more similar to PAAS concentrations, with the exception of Sr and Mo that are slightly enriched with respect to PAAS values in some samples (Fig. 4).

The ∑REE abundances in Amouslek Formation samples range from 15 to 171 $mg \cdot kg^{-1}$ (Table 2), while Igoudine Formation samples show low concentrations varying between 3 and 28 $mg \cdot kg^{-1}$. The clear positive correlation between ∑REE content and Th and Al (Fig. 5) suggests that the REEs are carried in mineral phases of the silt and clay fractions.

The non-marine, mainly detrital origin of the REE signature is further suggested by the PAAS normalized REE patterns, showing shapes similar to the typical shale pattern with flat REE distribution (Fig. 6), while the modern oxygenated seawater REE+Y PAAS normalized pattern is characterized by negative Ce anomaly, positive Y anomaly and high REE (HREE) enrichment (Shields and Webb 2004).

Even in the pure carbonate lithologies from the Igoudine and Amouslek formations (calcite and/or dolomite content > 95 wt%), the PAAS patterns are flat with a slight depletion in HREE. Furthermore, the Y/Ho ratios of the samples vary from 25 to 36, characteristic of crustal values (Table 2). Yttrium is geochemically similar to Ho, and chondritic materials and igneous rocks show a Y/Ho ratio of ca 28 (Bau and Dulski 1996). However, in oxygenated seawater, Ho is preferentially removed by Fe-Mn oxyhydroxides (Bau and Dulski 1994), driving the Y/Ho values in modern oceans above 52 (Nozaki et al. 1997).

Some of the studied samples show a positive Eu anomaly in the normalized patterns of shale (Fig. 8). During ICP-MS analysis, the formation of Ba oxide interferes with the Eu signal and can cause a false positive Eu anomaly (Kent and Ungerer 2005). However, there is no correlation between Eu/Eu* and Ba ($r^2 = 0.11$, $p > 0.10$), nor with the mineral composition (feldspars can potentially carry excess Ba) in the studied samples.

The chondrite-normalized REE patterns (Fig. 7) of the samples of the Amouslek and Igoudine formations exhibit similar shaped profiles with enrichments in the light REE (LREE), flat HREE, and weak negative Eu anomalies in most of the samples. The chondrite-normalized La_{CN}/Yb_{CN} ratios vary from 5.9 to 13.2 and from 5.5 to 26.3 in the Amouslek and Igoudine formations, respectively, showing fractionation and enrichment of the LREE. Also, the HREE is characterized by flat patterns with Gd_{CN}/Yb_{CN} values of 1.5–2.8 and 1.5–3.6 for the Amouslek and Igoudine formations, respectively (Table 2).

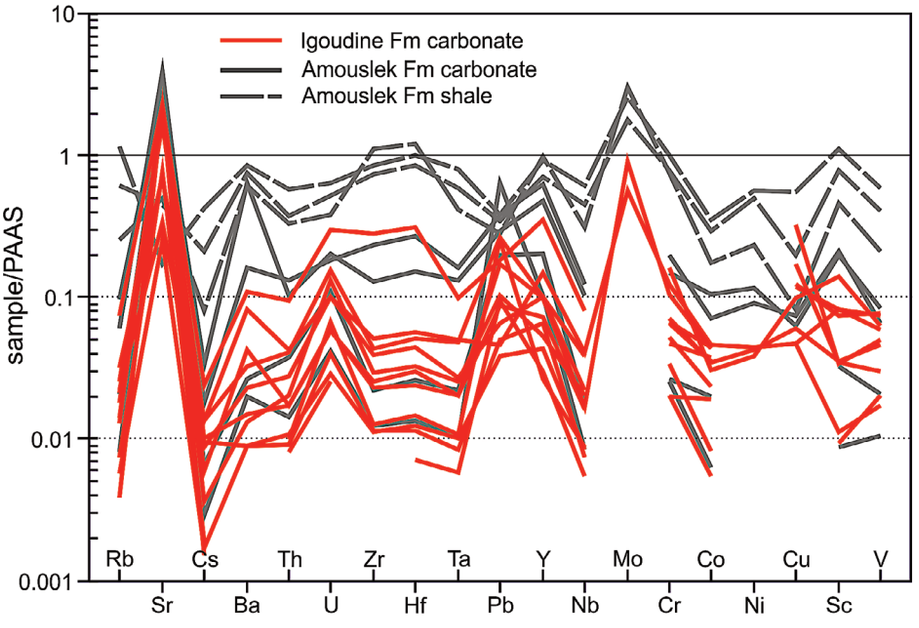

Fig. 4. PAAS (Taylor and McLennan 1985) normalized trace element distribution of samples from Igoudine carbonates (red line) and from Amouslek carbonates and calcareous shales (gray line). Fm – Formation.

Table 2. Trace element concentrations (mg·kg^{-1}) for Igoudine carbonates and Amouslek calcareous shales

Sample	Ig 1	Ig 2	Ig 3	Ig 4	Ig 5	Ig 6	Ig 7	Ig 8	Ig 9	Ig 10	Am 1	Am 2	Am 3	Am 4	Am 5	Am 6	Am 7	Am 8
La	1.04	1.88	2.39	1.60	1.72	5.90	3.65	3.08	2.92	0.63	10.46	33.22	25.35	11.45	20.06	14.76	2.91	6.28
Ce	2.10	4.84	4.31	3.01	4.21	11.11	7.62	5.04	6.49	1.25	22.27	72.41	55.54	25.24	55.99	35.89	6.67	18.95
Pr	0.24	0.66	0.49	0.34	0.54	1.40	0.88	0.61	0.78	0.15	2.70	8.46	6.40	3.53	6.32	4.32	0.65	1.59
Nd	0.91	2.73	1.81	1.28	2.24	5.31	3.37	2.28	3.05	0.60	10.66	32.30	24.36	15.02	26.60	18.05	2.60	6.04
Sm	0.18	0.67	0.33	0.25	0.51	1.02	0.65	0.38	0.62	0.13	2.04	6.10	4.70	3.42	6.08	3.98	0.51	1.25
Eu	0.04	0.14	0.08	0.07	0.11	0.23	0.13	0.11	0.15	0.03	0.67	1.23	0.95	0.90	1.32	0.97	0.13	0.32
Gd	0.15	0.58	0.30	0.22	0.42	0.86	0.55	0.35	0.52	0.13	1.81	4.89	3.93	2.99	5.51	3.55	0.51	1.11
Tb	0.02	0.09	0.04	0.03	0.07	0.12	0.08	0.05	0.08	0.02	0.26	0.75	0.59	0.45	0.85	0.53	0.07	0.16
Dy	0.13	0.55	0.24	0.17	0.39	0.72	0.48	0.26	0.47	0.11	1.52	4.63	3.60	2.59	5.11	3.09	0.43	0.94
Ho	0.03	0.10	0.05	0.03	0.07	0.14	0.10	0.05	0.09	0.02	0.30	0.97	0.73	0.48	0.99	0.59	0.09	0.18
Er	0.07	0.26	0.12	0.09	0.19	0.36	0.25	0.11	0.24	0.07	0.78	2.69	2.00	1.14	2.49	1.43	0.22	0.43
Tm	0.01	0.04	0.02	0.01	0.03	0.05	0.04	0.01	0.03	0.01	0.11	0.39	0.29	0.15	0.35	0.19	0.03	0.06
Yb	0.05	0.23	0.11	0.07	0.16	0.31	0.24	0.08	0.20	0.05	0.72	2.61	2.01	0.93	2.30	1.19	0.17	0.32
Lu	0.01	0.03	0.02	0.01	0.02	0.05	0.03	0.01	0.03	0.01	0.11	0.38	0.31	0.13	0.34	0.17	0.02	0.04
∑REE	4.96	12.81	10.31	7.18	10.67	27.58	18.07	12.41	15.68	3.22	54.41	171.03	130.76	68.43	134.29	88.73	15.01	37.67
Eu/Eu*	0.69	2.46	1.34	1.24	1.92	4.00	2.29	1.91	2.54	0.55	11.61	21.24	16.46	15.58	22.70	16.77	2.24	5.51
Co	0.44	1.00	0.54	0.19	1.03	1.06	0.82	0.87	0.79	0.13	0.71	8.10	6.71	2.40	4.03	1.64	0.14	0.46
Cr	2.21	11.50	5.80	3.70	7.40	13.63	7.22	5.17	7.86	2.24	17.76	111.02	86.24	16.32	83.39	21.69	2.81	2.92
Ni	–	–	–	–	–	2.43	–	–	2.35	–	2.12	31.22	27.33	6.35	12.81	5.02	–	–
V	2.59	7.46	4.50	2.01	11.66	8.88	11.09	3.04	6.97	1.31	9.35	89.01	61.45	12.59	31.41	9.91	1.58	3.13
Sr	155.26	410.17	414.09	424.65	410.38	140.51	339.64	51.16	67.56	437.91	470.40	34.72	91.02	527.98	99.27	788.27	481.16	487.12
Rb	1.19	2.24	2.07	2.86	3.41	5.09	4.11	0.92	3.54	0.61	11.90	184.69	98.00	15.50	40.66	9.58	1.30	3.30
Ba	–	9.74	8.50	5.80	27.56	53.14	21.36	5.79	14.97	–	70.74	557.77	493.73	417.55	397.42	105.60	12.93	17.24
Pb	5.06	3.47	2.05	0.76	1.74	0.92	5.32	1.01	1.30	1.88	3.67	7.73	6.85	5.90	5.68	7.74	12.81	3.96
Zr	2.65	5.39	6.17	2.36	4.85	10.76	9.20	2.41	8.27	–	59.53	179.71	155.40	27.00	232.97	49.45	2.60	4.67
Y	0.71	2.68	1.45	1.16	1.97	4.03	2.73	1.76	2.72	0.82	9.47	25.13	19.12	13.03	26.70	17.05	2.76	5.45
Nb	0.17	0.32	0.38	0.16	0.31	0.78	0.72	0.14	0.42	0.10	1.54	11.71	8.54	1.97	5.94	2.34	0.16	0.34
Hf	0.07	0.15	0.16	0.06	0.12	0.28	0.26	0.06	0.22	0.04	1.55	5.08	4.31	0.77	6.08	1.36	0.07	0.13

Ig – Igoudine, Am – Amouslek.

Continued on the next page

Table 2. *Continued*

Sample	Ig 1	Ig 2	Ig 3	Ig 4	Ig 5	Ig 6	Ig 7	Ig 8	Ig 9	Ig 10	Am 1	Am 2	Am 3	Am 4	Am 5	Am 6	Am 7	Am 8
Th	0.15	0.25	0.30	0.16	0.25	0.62	0.59	0.13	0.40	0.12	1.39	8.47	5.52	1.49	4.89	1.92	0.21	0.54
U	0.21	0.18	0.41	0.09	0.18	0.31	0.48	0.12	0.31	0.08	0.92	2.00	1.62	0.63	1.19	0.57	0.13	0.34
Cu	2.37	16.23	8.64	–	6.23	2.37	5.98	–	3.03	–	4.97	27.81	10.01	3.16	4.09	3.70	–	–
Sc	0.18	0.54	0.56	0.13	1.18	1.32	1.32	0.15	0.57	–	2.26	17.82	12.69	3.21	7.39	3.40	0.14	0.52
Zn	7.54	–	–	–	–	14.37	8.24	7.77	9.16	–	12.04	68.70	52.94	14.02	12.49	9.52	50.16	8.17
Mo	–	0.91	–	–	–	0.56	–	–	–	–	–	2.57	1.78	–	3.03	–	–	–
Th/Sc	0.81	0.46	0.53	1.20	0.21	0.47	0.45	0.89	0.71	–	0.61	0.48	0.43	0.46	0.66	0.57	1.50	1.05
Th/Co	0.33	0.25	0.55	0.83	0.24	0.58	0.72	0.15	0.51	0.93	1.95	1.05	0.82	0.62	1.21	1.17	1.45	1.19
La/Sc	5.79	3.48	4.27	12.28	1.46	4.47	2.76	20.56	5.13	–	4.63	1.86	2.00	3.57	2.71	4.34	20.78	12.08
Zr/Sc	14.70	9.99	11.02	18.13	4.11	8.15	6.97	16.07	14.51	–	26.34	10.08	12.25	8.41	31.53	14.54	18.59	8.97
U/Al	1.00	0.27	0.68	0.47	0.24	0.22	0.37	0.65	0.43	0.76	0.33	0.11	0.11	0.19	0.11	0.15	0.70	0.81
V/Al	12.53	11.01	7.52	10.44	15.40	6.27	8.63	16.01	9.79	12.70	3.39	5.04	4.33	3.78	2.83	2.67	8.58	7.37
Mo/Al	–	1.34	–	–	–	0.40	–	–	–	–	–	0.15	0.13	–	0.27	–	–	–
Y/Ho	27.88	25.77	31.21	35.39	26.41	29.21	28.19	35.88	29.11	34.36	31.39	25.95	26.17	27.34	26.91	28.98	31.13	30.69
La/Yb	19.15	8.19	21.68	23.31	10.55	18.92	15.23	38.93	14.45	12.11	14.47	12.74	12.60	12.28	8.73	12.39	16.65	19.46
Gd/Yb	2.79	2.54	2.74	3.22	2.57	2.74	2.30	4.45	2.58	2.46	2.50	1.88	1.95	3.20	2.40	2.98	2.89	3.43

Ig – Igoudine, Am – Amouslek.

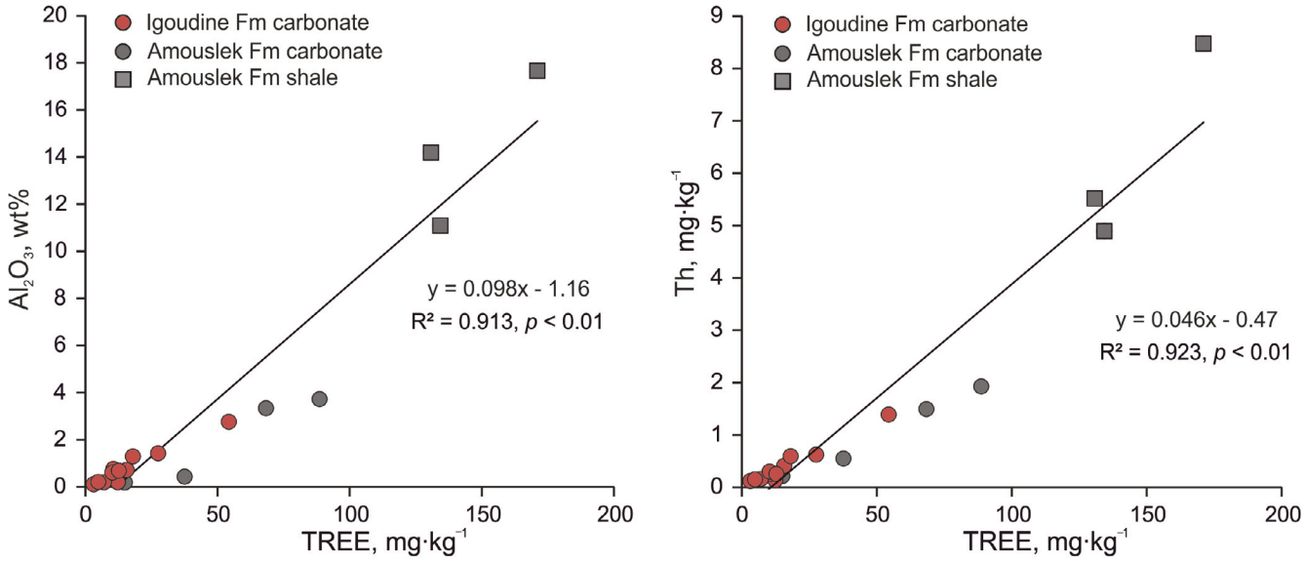

Fig. 5. Covariance in total REE and Al_2O_3 and Th content in the studied samples. Fm – Formation.

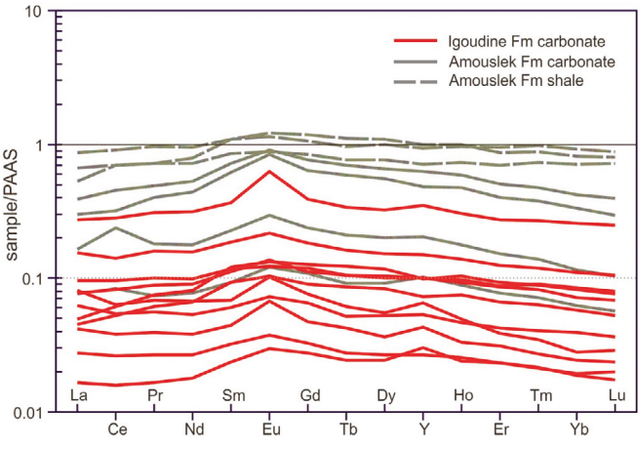

Fig. 6. PAAS (Taylor and McLennan 1985) normalized REE + Y patterns of Igoudine and Amouslek formation samples. Fm – Formation.

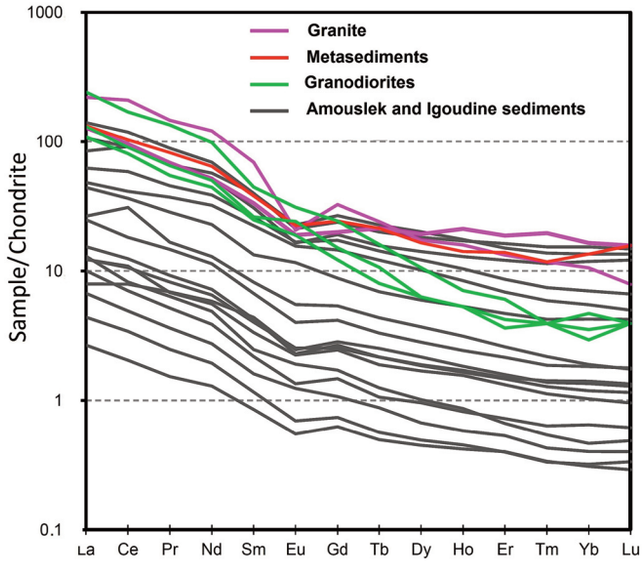

Fig. 7. Chondrite-normalized REE patterns of Igoudine and Amouslek samples, compared to plutonic rock and metasediment complexes in potential source areas (data from Barbey et al. 2001). Chondrite normalization values are from Taylor and McLennan (1985).

Discussion

Provenance of the terrigenous fraction

Major elements, trace elements, and rare earth element compositions carried by detrital phases allow the determination of the source rocks of detrital fraction (Cullers 1995; Madhavaraju and Ramasamy 2002; Armstrong-Altrin et al. 2004).

Hayashi et al. (1997) have shown that Al_2O_3/TiO_2 ratios range from 3 to 8 in mafic igneous rocks, increase to values ranging between 8 and 21 in intermediate rocks, and reach up to 70 in felsic igneous rocks. In the Igoudine Formation carbonates, Al_2O_3/TiO_2 ratios vary from 23 to 39.8, but are somewhat lower in calcareous shales of the Amouslek Formation, varying between 22.3 and 26.3 (Table 1). The Al_2O_3/TiO_2 ratios of the studied samples likely suggest the intermediate or mixed felsic (granite) and mafic (basalt) composition of the source rocks for the terrigenous fraction of sediments in the Igoudine and Amouslek formations (Fig. 8A), while the slightly higher Al_2O_3/TiO_2 ratio in the Igoudine Formation points to a more acidic source rock composition.

This interpretation is further supported by the Th/Co vs La/Sc plot (Cullers 2002; Fig. 8B), where the analyzed sedimentary rocks plot in the field of silicic (felsic) source rocks. The clear felsic source rock signature of the terrigenous fraction in the studied sediments is also evident from the LREE enrichment (elevated La_{CN}/Yb_{CN} ratios) and rather flat HREE segments in the chondrite-normalized REE patterns of both formations, and from the appearance of a negative Eu anomaly in most of the samples in chondrite-normalized REE patterns (Fig. 7). In addition, a few samples from both formations show the signature of sediment recycling and Zr

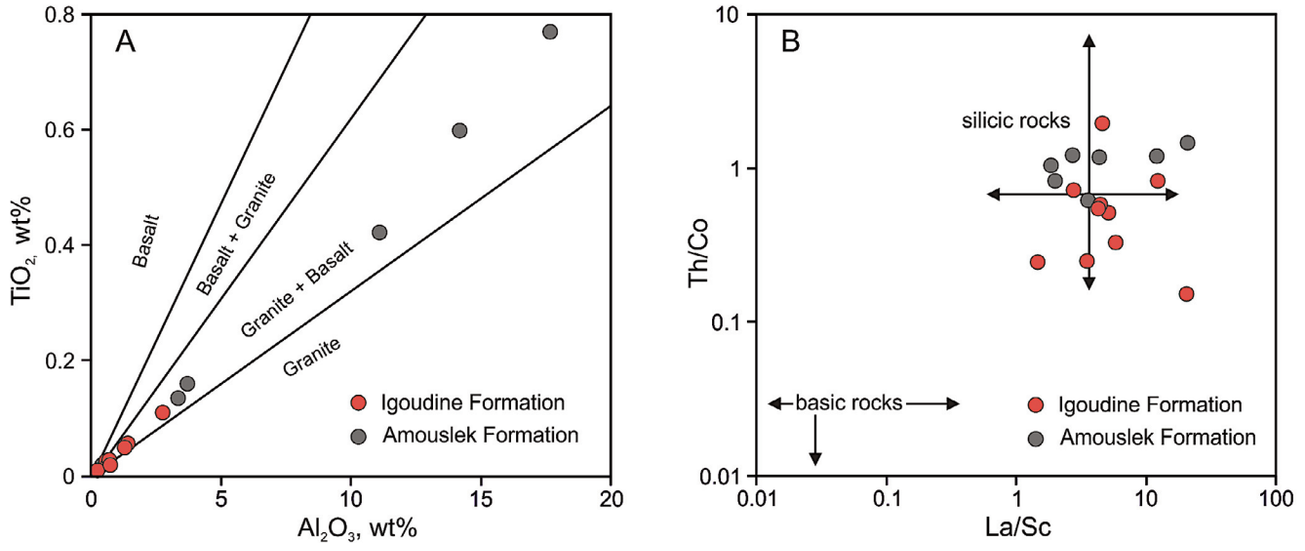

Fig. 8. Provenance discrimination diagrams for Igoudine and Amouslek samples. **A** – TiO_2 vs Al_2O_3 (Hayashi et al. 1997). **B** – Th/Co vs La/Sc (Cullers 2002).

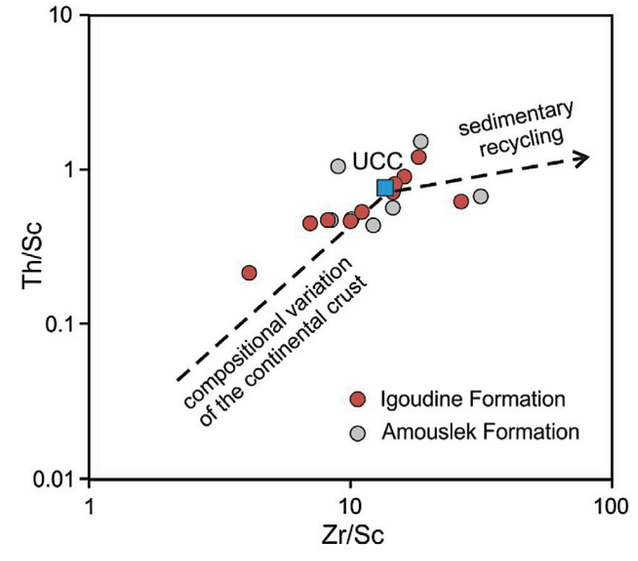

Fig. 9. Zr/Sc vs Th/Sc plot showing compositional variation in the sample sets and Zr addition in some samples. Composition of the upper continental crust (UCC) (Rudnick and Gao 2003) is marked with the blue box.

addition in the Th/Sc vs Zr/Sc plot (Fig. 9), whereas most of the samples plot close to the upper continental crust value, suggesting limited recycling and/or sedimentary sorting. Overall, the REE patterns of the samples from the Igoudine and Amouslek formations are comparable with those of Paleoproterozoic–Neoproterozoic granites and metasediments of Kerdous inliers (Barbey et al. 2001; Fig. 7), which could be considered possible source areas for the terrigenous fraction deposited in the shallow carbonate platform during the early Cambrian in the Anti-Atlas region.

Paleo-redox conditions

The content and ratios of several trace elements such as Mo, U, Cr, Ni, Co, V, and Mn are widely used as proxies for oxic, dysoxic, suboxic (anoxic-ferruginous) and euxinic paleoredox conditions, which are important for interpreting and understanding biogeochemical cycles (e.g. Breck 1974; Wignall and Myers 1988; Poulton and Canfield 2011; Algeo and Li 2020). Over the decades, several redox proxies have been developed to allow the distinction between deposits formed under oxic, dysoxic, suboxic, ferruginous and/or euxinic redox conditions using redox sensitive trace elements that tend to be enriched under reducing conditions (e.g. Hatch and Leventhal 1992; Jones and Manning 1994; Tribovillard et al. 2006). However, a recent critical re-evaluation of many trace element ratios has questioned their usability as universal paleoredox proxies (Algeo and Liu 2020). Instead, Algeo and Li (2020) and Bennett and Canfield (2020) have suggested that only Mo, U, Re as well as transition metal V are the meaningful elements for redox interpretation analysis with reasonably well differentiated redox thresholds for distinct redox conditions and depositional environments.

For the analyzed dataset, it is evident that the hydrogenous redox proxies (e.g. Ce anomaly) cannot be assessed even in the purest carbonate samples with the calcite or dolomite content of >95 wt%, where the trace element and REE signature is carried in the terrigenous fraction of the sediment. This is due to low REE concentrations in the carbonate phases masked by detrital phases and/or overprinting due to diagenetic processes (e.g. LREE recycling from the dissolution of Fe-Mn oxyhydroxides), which significantly mutes the seawater signatures (Caetano-Filho et al. 2018).

However, to estimate the degree of enrichment or depletion of redox sensitive trace elements in the terrigenous fraction of the sediments, the trace element values were normalized against Al (e.g. Bennett and Canfield 2020). The V, U, and Mo enrichment values are consistently low in both formations and are between 2.5 and 12.1, 0.1 and 0.5, and 0.1 and 1.0, respectively (Table 2, Fig. 10). Enrichment of these elements is characteristic of suboxic-anoxic (euxinic) depositional settings, where authigenic molybdenum is taken up as particle-reactive thiomolybdate (Tribovillard et al. 2012), whereas reduced uranium (Barnes and Cochran 1990) and vanadium (Wanty and Goldhaber 1992) become immobilized in insoluble reduced forms. Compared with the discrimi-

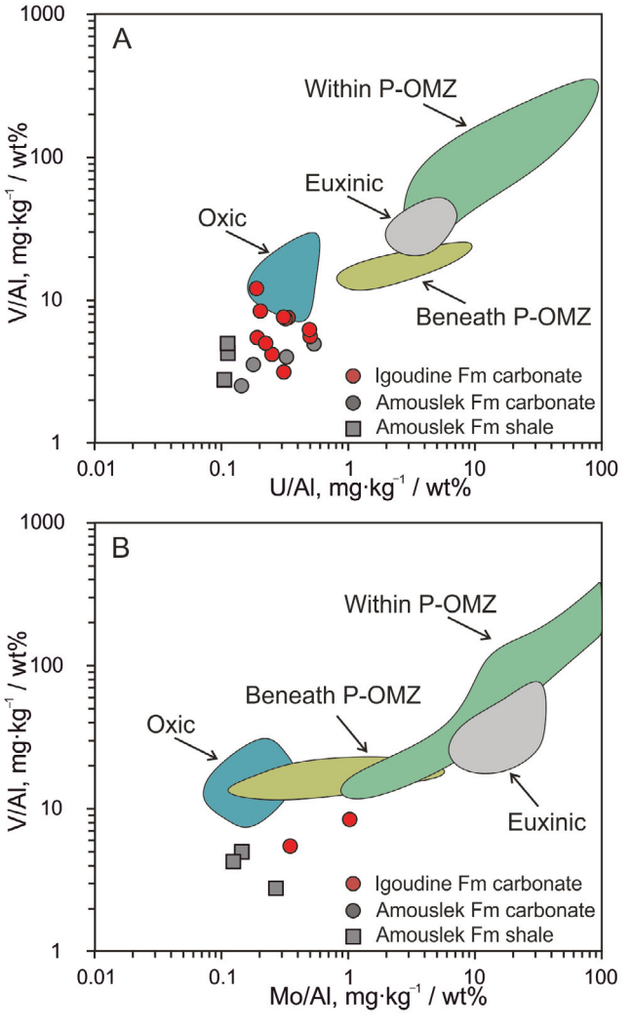

Fig. 10. Vanadium enrichments against uranium (A) and molybdenum (B) in the Amouslek and Igoudine formations. The fields for modern muds in oxic, euxinic basins, within and beneath perennial oxygen minimum zones (P-OMZ) are from Bennet and Canfield (2020). Fm – Formation.

nation of depositional conditions in the Bennett and Canfield (2020) compilation, most of the samples from the Amouslek and Igoudine formations plot outside the environmental fields defined by V/Al and Mo/Al ratios in modern marine muds (Fig. 10B). However, in the V/Al vs U/Al plot (Fig. 10A), the samples are in or close to the oxic field below the perennial oxygen minimum zone and the euxinic basin fields. In addition, although V and U enrichments show some variability in the sampled succession, the values stay within the range corresponding to the prevailing oxic depositional conditions (Fig. 11). Thus, our data show that the water column was prevailingly oxidized before, during and after the transition from the microbial consortium (stromatolite-dominated biota) to the thrombolite-archaeocyathan consortium and shelly metazoans at the Tommotian–Adtabanian (Cambrian Terreneuvian–Cambrian Epoch 2) boundary interval of the Anti-Atlas successions. This implies that the seawater redox status was not driving an important change in biological communities in these successions.

Indeed, although the final oxygenation of the atmosphere and ocean has been viewed in unison with the evolution of animal life, it has been shown that elevated oxygen was not the driving cause for animals to evolve (Knoll and Carroll 1999; Cole et al. 2020). The first fossil evidence for metazoans (sponges) dates back to as early as ca 890 Ma in the Tonian age (Turner 2021), when oxygen levels were only starting to rise (Wang et al. 2015). Moreover, the Cambrian explosion, defined as multi-phased rapid diversification of metazoans and their body plans coupled with progressive increase in ecosystem complexity, was not a single-step change but occurred during the first 20 million years of the Cambrian Period (Zhang and Shu 2021). On the one hand, a rise in oceanic oxygen has been suggested to partially explain the emergence of the Cambrian explosion (e.g. Sperling et al. 2015), on the other hand, the ocean water column redox was highly variable but mainly anoxic in the late Ediacaran and

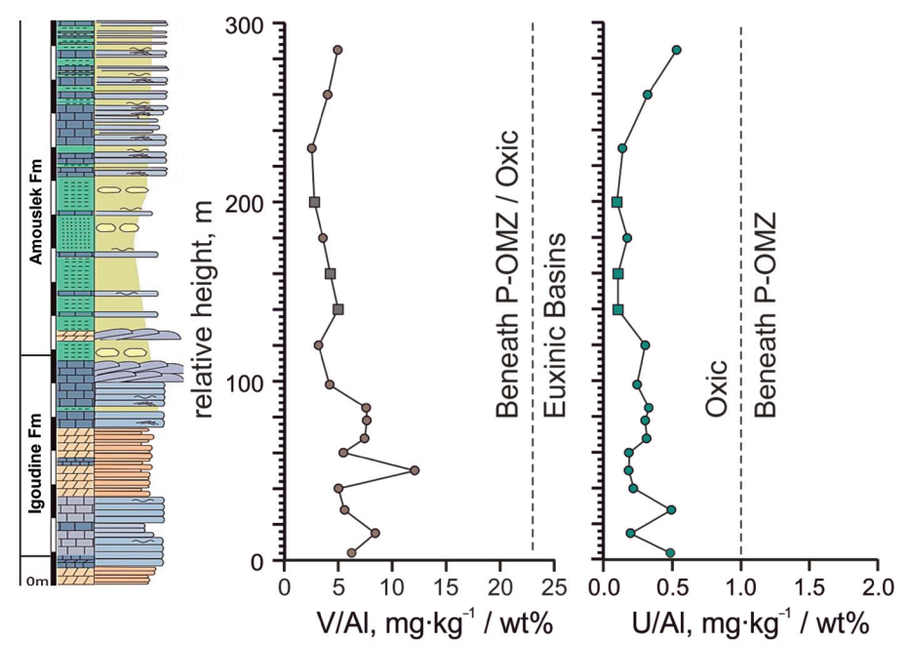

Fig. 11. V and U enrichment of sediments of the Igoudine and Amouslek formations in the Fouanou syncline (paleoredox condition boundaries from Bennet and Canfield 2020). Samples marked with squares are shales, circles denote carbonate-dominated samples.

early Cambrian (Wei et al. 2018; Tostevin et al. 2019). Zhang and Shu (2021) have recently reviewed the current state of understanding the causal mechanisms of the Cambrian explosion, and no single environmental nor biological cause can explain this phenomenon.

In the western Anti-Atlas, the onset of thrombolites-archaeocyathan reefs and shelly metazoans succeeded stromatolite consortia in a transgressive context (Álvaro et al. 2003; Clausen et al. 2014). Clausen et al. (2014) have suggested that the main control on the diversity and migration of archaeocyaths and shelly metazoans was the early Cambrian (Cambrian Epoch 2, Age 3) emergence of open marine conditions, facilitated by differential subsidence of the platform and a long-term sea-level rise. Cambrian Age 3–4 intervals are characterized by a peak in carbonate productivity in relation to a globally warm climate. Recent reconstructions of the early-Cambrian paleogeography place the Anti-Atlas at paleolatitudes of about 25–35° S, suggesting a warm and semi-arid climate (Álvaro et al. 2000, 2003; Clausen et al. 2014). The delayed records of shelly metazoans in the Anti-Atlas basins could be explained by the restricted connection with the open ocean realm, limiting the immigration of metazoans but promoting the establishment of microbial ecosystems.

Conclusions

This study shows that the lower Cambrian Igoudine Formation limestone-dolomite succession of the Anti-Atlas is dominated by calcite or dolomite composition with small amounts of quartz, K-feldspar, plagioclase, and phyllosilicate. The lower part of the succeeding Amouslek Formation, represented by shales and siltstones, is characterized by quartz–feldspar and phyllosilicate assemblages, whereas the upper parts of this formation are dominated by carbonate minor quartz, feldspar and phyllosilicates.

Discrimination diagrams of the source rocks based on major elements and trace elements (Th/Co versus La/Sc, TiO_2 versus Al_2O_3 and Th/Sc versus Zr/Sc), chondrite-normalized REE patterns of carbonate and calcareous shale samples further indicate that the sediments were likely derived from weathering and erosion of predominantly felsic rocks that can be tied to Paleo-Neoproterozoic granites and metasediments of the Kerdous inlier.

Redox proxies such as U/Al and V/Al suggest that the Igoudine and the Amouslek formations of the Anti-Atlas successions were deposited in the oxic environment. This implies that the seawater oxygenation status was not driving the biological replacement of microbial consortium (stromatolite-dominated biota) by a thrombolite-archaeocyathan consortium and shelly metazoans in the western Anti-Atlas, but was controlled by a restricted connection to the open sea, which promoted the evolution of microbial ecosystems.

Acknowledgments

Financial support for this study was provided by the Académie Hassan II des Sciences et Techniques, Morocco, and the region Nouvelle Aquitaine. The authors are grateful to Lhoussain Ablouh (Centre des Analyses Chimique, UCA, France) and Emile Béré (UFR SFA, Pole IMAGE UP, University of Poitiers, France) for technical support with SEM and EDX analyses. Mouad Akboub, Idir Elhabib, and Mouhssin Elhalim are thanked for their assistance during the field work. Leho Ainsaar and an anonymous reviewer are acknowledged for their constructive comments. The analyses at the University of Tartu, Estonia, were supported by the Estonian Centre of Analytical Chemistry. The publication costs of this article were covered by the Estonian Academy of Sciences.

References

Alcott, L. J., Mills, B. J. W. and Poulton, S. W. 2019. Stepwise Earth oxygenation is an inherent property of global biogeochemical cycling. *Science*, **366**, 1333–1337.

Algeo, T. J. and Li, C. 2020. Redox classification and calibration of redox thresholds in sedimentary systems. *Geochimica et Cosmochimica Acta*, **287**, 8–26.

Algeo, T. J. and Liu, J. S. 2020. A re-assessment of elemental proxies for paleoredox analysis. *Chemical Geology*, **540**, 119549.

Álvaro, J. J. and Clausen, S. 2006. Microbial crusts as indicators of stratigraphic diastems in the Cambrian Brèche à *Micmacca*, Atlas Mountains of Morocco. *Sedimentary Geology*, **185**, 255–265.

Álvaro, J. J. and Debrenne, F. 2010. The Great Atlasian Reef Complex: an early Cambrian subtropical fringing belt that bordered West Gondwana. *Palaeogeography, Palaeoclimatology, Palaeoecology*, **294**, 120–132.

Álvaro, J. J., Rouchy, J. M., Bechstädt, T., Boucot, A., Boyer, F., Debrenne, F. et al. 2000. Evaporitic constraints on the southward drifting of the western Gondwana margin during Early Cambrian times. *Palaeogeography, Palaeoclimatology, Palaeoecology*, **160**, 105–122.

Álvaro, J. J., Elicki, O., Geyer, G., Rushton, A. W. A. and Shergold, J. H. 2003. Palaeogeographical controls on the Cambrian trilobite immigration and evolutionary patterns reported in the western Gondwana margin. *Palaeogeography, Palaeoclimatology, Palaeoecology*, **195**, 5–35.

Álvaro, J. J., Benziane, F., Thomas, R., Walsh, G. J. and Yazidi, A. 2014. Neoproterozoic–Cambrian stratigraphic framework of the Anti-Atlas and Ouzellagh promontory (High Atlas), Morocco. *Journal of African Earth Sciences*, **98**, 19–33.

Amthor, J., Grotzinger, J., Schröder, S., Bowring, S., Ramezani, J., Martin, M. et al. 2003. Extinction of Cloudina and Namacalathus at the Precambrian–Cambrian boundary in Oman. *Geology*, **31**, 431–434.

Armstrong-Altrin, J. S., Lee, Y. I., Verma, S. P. and Ramasamy, S. 2004. Geochemistry of sandstones from the upper Miocene Kudankulam Formation, Southern India: Implications for provenance, weathering and tectonic setting. *Journal of Sedimentary Research*, **74**, 285–297.

Azizi, A., El Albani, A., El Bakhouche, A., Vinn O., Bankole, O. M., Fontaine, C. et al. 2022. *Early Biomineralization and Exceptional Preservation of the First Thrombolite Reefs with Archaeocyaths in the Lower Cambrian of the Western Anti-Atlas, Morocco*. Cambridge University Press. https://doi.org/10.1017/S0016756822001017

Barbey, P., Nachit, H. and Pons, J. 2001. Magma–host interactions during differentiation and emplacement of a shallow-level, zoned granitic pluton (Tarçouate pluton, Morocco): implications for magma emplacement. *Lithos*, **58**, 125–143.

Barnes, C. E. and Cochran, J. K. 1990. Uranium removal in oceanic sediments and the oceanic U balance. *Earth and Planetary Science Letters*, **97**, 94–101.

Bau, M. and Dulski, P. 1994. Evolution of the yttrium-holmium systematics of seawater through time. *Mineralogical Magazine*, **58A**, 61–62.

Bau, M. and Dulski, P. 1996. Distribution of yttrium and rare-earth elements in the Penge and Kuruman iron-formations, Transvaal Supergroup, South Africa. *Precambrian Research*, **79**, 37–55.

Bennett, W. W. and Canfield, D. E. 2020. Redox-sensitive trace metals as paleoredox proxies: A review and analysis of data from modern sediments. *Earth-Science Reviews*, **204**, 103175.

Benssaou, M. and Hamoumi, N. 2001. L'Anti-Atlas occidental du Maroc: étude sédimentologique et reconstitutions paléogéographiques au Cambrien inférieur (The western Anti-Atlas of Morocco: sedimentological study and paleogeographic reconstructions in the Lower Cambrian). *Journal of African Earth Sciences*, **32**, 351–372.

Benssaou, M. and Hamoumi, N. 2004. Les microbialites de l'Anti-Atlas occidental (Maroc): marqueurs stratigraphiques et témoins des changements environnementaux au Cambrien inférieur (Stratigraphic and environmental significance of the Lower-Cambrian western Anti-Atlasic microbialites (Morocco)). *Comptes Rendus Geosciences*, **336**, 109–116.

Brasier, M. D. 1982. Sea-level changes, facies changes and the late Precambrian–early Cambrian evolutionary explosion. *Precambrian Research*, **17**, 105–123.

Breck, W. G. 1974. Redox levels in the sea. In *The Sea: Ideas and Observations on Progress in the Study of the Seas, Marine Chemistry* (Goldberg, E. D., ed.). Wiley, New York, **5**, 153–179.

Buggisch, W. and Flügel, E. 1988. The Precambrian/Cambrian boundary in the Anti-Atlas (Morocco) discussions and new results. In *The Atlas System of Morocco. Studies on its Geodynamic Evolution* (Jacobshagen, V. H., ed.). *Lecture Notes in Earth Sciences*, **15**, 81–90.

Buggisch, W. and Heinitz, W. 1984. Slumpfolds and other early deformations in the early Cambrian of the Western and Central Anti-Atlas (Morocco). *Geologische Rundschau*, **73**, 809–818.

Butterfield, N. J. 2015. Early evolution of the Eukaryota. *Palaeontology*, **58**, 5–17.

Caetano-Filho, S., Paula-Santos, G. M. and Dias-Brito, D. 2018. Carbonate REE + Y signatures from the restricted early marine phase of South Atlantic Ocean (late Aptian–Albian): The influence of early anoxic diagenesis on shale-normalized REE + Y patterns of ancient carbonate rocks. *Palaeogeography, Palaeoclimatology, Palaeoecology*, **500**, 69–83.

Choubert, G. 1952. Histoire géologique du domaine de l'Anti-Atlas (Geological history of the Anti-Atlas region). In *Géologie du Maroc. XIXe Congrès Géologique International: Monographies Régionales, 3e Série: Maroc* (*Geology of Morocco. The 19th International Geological Congress: Regional Monographs, 3rd Series: Morocco*) (Choubert, G. and Marçais, J., eds), No. 6, 77–194.

Clausen, S., Álvaro, J. J. and Zamora, S. 2014. Replacement of benthic communities in two Neoproterozoic–Cambrian subtropical-to-temperate rift basins, High Atlas and Anti-Atlas, Morocco. *Journal of African Earth Sciences*, **98**, 72–93.

Cole, D. B., Mills, D. B., Erwin, D. H., Sperling, E. A., Porter, S. M., Reinhard, C. T. et al. 2020. On the co-evolution of surface oxygen levels and animals. *Geobiology*, **18**, 260–281.

Cullers, R. L. 1995. The controls on the major- and trace-element evolution of shales, siltstones and sandstones of Ordovician to Tertiary age in the Wet Mountain region, Colorado, U.S.A. *Chemical Geology*, **123**, 107–131.

Cullers, R. L. 2002. Implications of elemental concentrations for provenance, redox conditions, and metamorphic studies of shales and limestones near Pueblo, CO, USA. *Chemical Geology*, **191**, 305–327.

Debrenne, F. and Debrenne, M. 1995. Archaeocyaths of the Lower Cambrian of Morocco. *Beringeria*, **2**, 121–145.

Destombes, J., Hollard, H. and Willefert, S. 1985. Lower Palaeozoic rocks of Morocco. In *Lower Palaeozoic Rocks of the World. Lower Palaeozoic of North-Western and West Central Africa* (Holland, C. H., ed.). John Wiley and Sons, Chichester, **4**, 91–336.

Ducrot, J. and Lancelot, J. R. 1977. Problème de la limite Précambrien–Cambrien: étude radiochronologique par la méthode U/Pb sur zircon du volcan du Jbel Boho (Precambrian–Cambrian boundary problem: radiochronological study using the U/Pb method on zircon from the Jbel Boho volcano). *Canadian Journal of Earth Sciences*, **14**, 1771–1777.

Gasquet, D., Levresse, G., Cheilletz, A., Azizi-Samir, M. R. and Mouttaqi, A. 2005. Contribution to a geodynamic reconstruction of the Anti-Atlas (Morocco) during Pan-African times with the emphasis on inversion tectonics and metallogenic activity at the Precambrian–Cambrian boundary. *Precambrian Research*, **140**, 157–182.

Gasquet, D., Ennih, N., Liégeois, J. P., Soulaimani, A. and Michard, A. 2008. The Pan-African belt. In *Continental Evolution: The Geology of Morocco. Structure, Stratigraphy, and Tectonics of the African-Atlantic-Mediterranean Triple Junction* (Michard, A., Chalouan, A., Saddiqi, O. and de Lamotte, D., eds). *Lecture Notes in Earth Sciences*, **116**, 33–64.

Geyer, G. and Landing, E. (eds). 1995. Morocco '95. The Lower–Middle Cambrian standard of Gondwana. *Beringeria*, **2**, 1–171.

Grotzinger, J. and Knoll, A. 1995. Anomalous carbonate precipitates: is the Precambrian the key to the Permian? *Palaios*, **10**, 578–596.

Halverson, G. P. and Shields-Zhou, G. 2011. Chemostratigraphy and the Neoproterozoic glaciations. *Geological Society, London, Memoirs*, **36**, 51–66.

Harland, W. B. 2007. Origins and assessment of snowball Earth hypotheses. *Geological Magazine*, **144**, 633–642.

Hatch, J. R. and Leventhal, J. S. 1992. Relationship between inferred redox potential of the depositional environment and geochemistry of the Upper Pennsylvanian (Missourian) Stark Shale Member of the Dennis Limestone, Wabaunsee County, Kansas, U.S.A. *Chemical Geology*, **99**, 65–82.

Hayashi, K., Fujisawa, H., Holland, H. and Ohmoto, H. 1997. Geochemistry of ~1.9 Ga sedimentary rocks from northeastern Labrador, Canada. *Geochimica et Cosmochimica Acta*, **61**, 4115–4137.

Hoffman, P. F., Abbot, D. S., Ashkenazy, Y., Benn, D. I., Brocks, J. J., Cohen, P. A. et al. 2017. Snowball Earth climate dynamics and Cryogenian geology-geobiology. *Science Advances*, **3**, 1600983.

Hupé, P. 1960. Sur le Cambrien inférieur du Maroc (On the Lower Cambrian of Morocco). In *Reports of the 21st International Geological Congress*, **8**, 75–85.

Jones, B. and Manning, D. A. C. 1994. Comparison of geochemical indices used for the interpretation of palaeoredox conditions in ancient mudstones. *Chemical Geology*, **111**, 111–129.

Kent, A. J. R. and Ungerer, C. A. 2005. Production of barium and light rare earth element oxides during LA-ICP-MS micro-analysis. *Journal of Analytical Atomic Spectrometry*, **20**, 1256–1262.

Kimura, H. and Watanabe, Y. 2001. Ocean anoxia at the Precambrian–Cambrian boundary. *Geology*, **29**, 995–998.

Knoll, A. and Carroll, S. 1999. Early animal evolution: Emerging views from comparative biology and geology. *Science*, **284**, 2129–2137.

Lawrence, M. G., Collerson, K. D. and Kamber, B. S. 2006. Significance of the longevity of the marine rare earth pattern. *Geochimica et Cosmochimica Acta*, **70**, A345.

Levinton, J. S. 2008. The Cambrian Explosion: How do we use the evidence. *BioScience*, **58**, 855–864.

Madhavaraju, J. and Ramasamy, S. 2002. Petrography and geochemistry of Late Maastrichtian – Early Paleocene sediments of Tiruchirapalli Cretaceous, Tamil Nadu – paleoweathering and provenance implications. *Journal of the Geological Society of India*, **59**, 133–142.

Maloof, A. C., Schrag, D. P., Crowley, J. L. and Bowring, S. A. 2005. An expanded record of early Cambrian carbon cycling for the Anti-Atlas margin, Morocco. *Canadian Journal Earth Sciences*, **42**, 2195–2216.

Narbonne, G. M. 2005. The Ediacara biota: Neoproterozoic origin of animals and their ecosystems. *Annual Review of Earth and Planetary Sciences*, **33**, 421–442.
Nozaki, Y., Zhang, J. and Amakawa, H. 1997. The fractionation between Y and Ho in the marine environment. *Earth and Planetary Science Letters*, **148**, 329–340.
Och, L. M. and Shields-Zhou, G. A. 2012. The Neoproterozoic oxygenation event: Environmental perturbations and biogeochemical cycling. *Earth-Science Reviews*, **110**, 26–57.
Poulton, S. W. and Canfield, D. E. 2011. Ferruginous conditions: a dominant feature of the ocean through Earth's history. *Elements*, **7**, 107–112.
Rowland, S. M. and Shapiro, R. S. 2002. Reef patterns and environmental influences in the Cambrian and earliest Ordovician. In *Phanerozoic Reef Patterns* (Kiessling, W., Flügel, E. and Golonka, J., eds). *SEPM Speciale Publication*, **72**, 95–128.
Rudnick, R. L. and Gao, S. 2003. Composition of the continental crust. In *Treatise on Geochemistry* (Holland, H. D. and Turekian, K. K., eds). Elsevier, Amsterdam, **3**, 1–64.
Saadi, S., Hilali, E., Bensaïd, M., Boudda, A. and Dahmani, M. 1985. Carte Géologique de Maroc: Rabat, Morocco, Ministère du l'Énergie et des Mines, Service Géologique du Maroc, scale 1:1,000,000 (Geological Map of Morocco: Rabat, Morocco, Ministry of Energy and Mines, Geological Service of Morocco, scale 1:1,000,000).
Schmitt, M. 1979. The Section of Tiout (Precambrian/Cambrian Boundary Beds, Anti-Atlas, Morocco): Stromatolites and their Biostratigraphy. *Arbeiten aus dem Paläontologischen Institut Würzburg*, **2**.
Schmitt, M. and Monninger, W. 1977. Stromatolites and thrombolites in Precambrian/Cambrian boundary beds of the Anti-Atlas, Morocco: preliminary results. In *Fossil Algae* (Flügel, E., ed.). Springer, Berlin, Heidelberg, 80–85.
Sdzuy, K. 1978. The Precambrian–Cambrian boundary beds in Morocco (Preliminary Report). *Geological Magazine*, **115**, 83–94.
Shields, G. A. and Webb, G. E. 2004. Has the REE composition of seawater changed over geological time? *Chemical Geology*, **204**, 103–107.
Smith, M. P. and Harper, D. A. T. 2013. Causes of the Cambrian Explosion. *Science*, **341**, 1355–1356.
Sperling, E. A., Knoll, A. H. and Girguis, P. R. 2015. The ecological physiology of Earth's second oxygen revolution. *Annual Review of Ecology, Evolution, and Systematics*, **46**, 215–235.
Taylor, S. R. and McLennan, S. M. 1985. *The Continental Crust: Its Composition and Evolution*. Blackwell, Oxford.
Thomas, R. J., Chevallier, L. P., Gresse, P. G., Harmer, R. E., Eglington, B. M., Armstrong, R. A. et al. 2002. Precambrian evolution of the Sirwa Window, Anti-Atlas Orogen, Morocco. *Precambrian Research*, **118**, 1–57.
Thomas, R. J., Fekkak, A., Ennih, N., Errami, E., Loughlin, S. C., Gresse, P. G. et al. 2004. A new lithostratigraphic framework for the Anti-Atlas Orogen, Morocco. *Journal of African Earth Sciences*, **39**, 217–226.
Tostevin, R., Clarkson, M. O., Gangl, S., Shields, G. A., Wood, R. A., Bowyer, F. et al. 2019. Uranium isotope evidence for an expansion of anoxia in terminal Ediacaran oceans. *Earth and Planetary Science Letters*, **506**, 104–112.
Tribovillard, N., Algeo, T. J., Lyons, T. and Riboulleau, A. 2006. Trace metals as paleoredox and paleoproductivity proxies: An update. *Chemical Geology*, **232**, 12–32.
Tribovillard, N., Algeo, T. J., Baudin, F. and Riboulleau, A. 2012. Analysis of marine environmental conditions based on molybdenum-uranium covariation – applications to Mesozoic paleoceanography. *Chemical Geology*, **324**, 46–58.
Tucker, M. E. 1986. Carbon isotope excursions in Precambrian/Cambrian boundary beds, Morocco. *Nature*, **319**, 48–50.
Turner, E. C. 2021. Possible poriferan body fossils in early Neoproterozoic microbial reefs. *Nature*, **596**, 87–91.
Walsh, G. J., Benziane, F., Aleinikoff, J. N., Harrison, R. W., Yazidi, A., Burton, W. C. et al. 2012. Neoproterozoic tectonic evolution of the Jebel Saghro and Bou Azzer–El Graara inliers, eastern and central Anti-Atlas, Morocco. *Precambrian Research*, **216–219**, 23–62.
Wang, S., Zou, C., Dong, D., Wang, Y., Li, X., Huang, J. et al. 2015. Multiple controls on the paleoenvironment of the Early Cambrian marine black shales in the Sichuan Basin, SW China: Geochemical and organic carbon isotopic evidence. *Marine and Petroleum Geology*, **66**, 660–672.
Wanty, R. B. and Goldhaber, M. B. 1992. Thermodynamics and kinetics of reactions involving vanadium in natural systems – accumulation of vanadium in sedimentary rocks. *Geochimica et Cosmochimica Acta*, **56**, 1471–1483.
Wei, G. Y., Planavsky, N. J., Tarhan, L. G., Chen, X., Wei, W., Li, D. et al. 2018. Marine redox fluctuation as a potential trigger for the Cambrian explosion. *Geology*, **46**, 587–590.
Wignall, P. B. and Myers, K. J. 1988. Interpreting benthic oxygen levels in mudrocks: a new approach. *Geology*, **16**, 452–455.
Wood, R., Liu, A. G., Bowyer, F., Wilby, P. R., Dunn, F. S., Kenchington, C. G. et al. 2019. Integrated records of environmental change and evolution challenge the Cambrian Explosion. *Nature Ecology & Evolution*, **3**, 528–538.
Zhang, X. L. and Shu, D. G. 2021. Current understanding on the Cambrian Explosion: questions and answers. *PalZ*, **95**, 641–660.

Maroko lääne Anti-Atlase vara-Kambriumi läbilõike geokeemia. Vihjed päritolule ja paleo-redokstingimustele

Abdelfattah Azizi, Abderrazak El Albani, Khadija El Hariri, Asmaa El Bakhouch, Olev Vinn, Ahmid Hafid ja Kalle Kirsimäe

Igoudine ja Amouslek kihistud (Terreneuvi ja Kambriumi teise ladestiku piiril) Maroko lääne Anti-Atlases kajastavad stromatoliite sisaldavate komplekside asendumist tromboliitide-hulkraksete kooslustega. Mõlema kihistu karbonaatseid kivimeid ja karbonaatseid argilliite on uuritud põhielementide, jälgelementide ning haruldaste muldmetallide osas, et hinnata terrigeense fraktsiooni päritolu ja paleo-redokstingimusi. Põhielementidel ja valitud jälgelementidel põhinevad lähtekivimite eristusdiagrammid näitavad, et setete terrigeensed fraktsioonid pärinevad tõenäoliselt valdavalt ränidioksiidirikastest kivimitest ning lähtekivimiteks olid Paleoproterosoikumi-Neoproterosoikumi graniidid ja Kerdouse piirkonna setted. Paleo-redokstingimuste indikaatorid nagu U / Al, V / Al ja Mo / Al viitavad sellele, et Igoudine ja Amouslek kihistute settimine toimus hapnikurikkas keskkonnas. Uuringu tulemused näitavad, et kohalik veemass oli hapnikurikas juba enne üleminekut mikroobide kogumike (stromatoliidid) domineeritud elustikult tromboliitide-arheotsüaatide kooslusele. See tähendab, et merevee redoksseisund ei põhjustanud bioloogiliste koosluste muutust.